Mixed Layer Temperature Balance on Intraseasonal Timescales in the Equatorial Pacific Ocean*

MICHAEL J. MCPHADEN

NOAA/Pacific Marine Environmental Laboratory, Seattle, Washington

(Manuscript received 12 November 2001, in final form 8 April 2002)

ABSTRACT

The purpose of this study is to document the zonal evolution of processes affecting sea surface temperature (SST) variability on intraseasonal timescales in the equatorial Pacific Ocean. Data primarily from the Tropical Atmosphere Ocean (TAO) array of moored buoys are used, focusing on four sites along the equator with decade-long time series. These sites are located in the western Pacific warm pool (165°E), the eastern Pacific equatorial cold tongue (110° and 140°W), and the transition zone between these two regions (170°W). Results indicate that SST variability on intraseasonal timescales is most significantly influenced by local surface heat fluxes in the western Pacific (165°E), zonal advection in the central Pacific (170°W), and vertical advection and entrainment in the eastern Pacific (110° and 140°W). East of the date line, oceanic equatorial Kelvin waves strongly mediate dynamical processes controlling intraseasonal SSTs variations, while surface fluxes tend to damp these dynamically generated SSTs at a rate of about 20 W m^{-2} $°C^{-1}$. The details of coupling between Kelvin wave dynamics and mixed layer processes make for complicated SST phasing along the equator. While thermocline temperatures propagate eastward at Kelvin wave speeds in the central and eastern Pacific, SSTs can develop in phase over thousands of kilometers, or may even appear to propagate westward. Implications of these results for understanding the dynamical connection between intraseasonal and interannual variability are discussed.

1. Introduction

In this study we examine the processes responsible for intraseasonal variations in sea surface temperature (SST) in the tropical Pacific Ocean. These variations are the result of atmospheric forcing associated with synoptic-scale weather phenomena in the western Pacific such as westerly wind bursts, cold air outbreaks from higher latitudes, and the Madden–Julian oscillation (MJO). The MJO, a wavelike phenomena with energy concentrated in a broad band of periods between about 30 and 90 days, is a particularly pronounced mode of atmospheric variability that affects surface winds and deep convection coherently over thousands of kilometers near the equator (Madden and Julian 1994). The MJO originates over the Indian Ocean and subsequently propagates eastward into the western Pacific, substantially modulating air–sea interactions over warm surface waters above 27°–28°C. Strong surface westerly winds, heavy rainfall, and reduced insolation are associated with convectively active phases of the MJO, during which the ocean cools locally in the western Pacific. In addition, westerly winds associated with the MJO generate downwelling equatorial Kelvin waves that propagate eastward across the basin in 1–2 months, affecting sea level, upper-ocean currents, and upper-ocean temperature structures along the way (Kessler et al. 1995; Hendon et al. 1998; McPhaden and Yu 1999).

Intraseasonal atmospheric variability represents a form of stochastic forcing of the climate system that may affect the intensity, frequency, and duration of ENSO warm and cold events (Kirtman and Schopf 1998; Moore and Kleeman 1999; Zhang et al. 2001). The 1997/98 El Niño provided a particularly striking example of intraseasonal influences on ENSO, with energetic MJO variations contributing to an unexpectedly rapid SST warming in early 1997 and a sudden cooling in mid-1998 in the equatorial Pacific (McPhaden 1999; Takayabu et al. 1999). The precise mechanisms by which intraseasonal variations may rectify into lower-frequency dynamics has been the subject of several studies (e.g., Harrison and Schopf 1984; Lukas and Lindstrom 1991; Kessler et al. 1995; Ralph et al. 1997; Kessler and Kleeman 2000; Zhang 2001), all of which involve some form of SST feedback to the atmosphere. Intraseasonal SST variations in the equatorial Pacific are typically $O(0.1°C)$ and generally small relative to those occurring on seasonal-to-interannual timescales.

* Joint Insitute for the Study of the Atmosphere and Ocean Contribution Number 887 and Pacific Marine Environmental Laboratory Contribution Number 2433.

Corresponding author address: Michael McPhaden, NOAA/Pacific Marine Environmental Laboratory, 7600 Sand Point Way NE, Seattle, WA 98115.
E-mail: mcphaden@pmel.noaa.gov

However, the atmosphere responds nonlinearly to small temperature changes when absolute temperatures are high. Thus, intraseasonal variations in SST need to be considered for a complete understanding of climate variability originating in the Tropics.

Intraseasonal variations in SST are also important for understanding variability associated with the MJO itself. A well-known shortcoming of atmospheric general circulation models is their inability to accurately simulate aspects of MJO variability. Modeled intraseasonal atmospheric variations often have periods that are too short, phase speeds that are too fast, and convection patterns that are not as highly organized as in observations (Slingo et al. 1996). Several recent studies suggest that allowing for interactive SSTs on intraseasonal timescales can improve the simulation of MJO variability through dynamical feedbacks to the atmosphere (Flatau et al. 1997; Wang and Xie 1998; Waliser et al. 1999a). A more accurate representation of MJO variability in atmospheric models leads to the possibility of improved dynamical predictions of the MJO and its effects on weather variability both in the Tropics and extratropics (Higgins and Mo 1997). These improvements in model representations of the MJO may also lead to improvements in the predictability of ENSO, to the extent that the MJO can influence the evolution of year-to-year climate variations.

The purpose of this study is therefore to diagnose the mechanisms responsible for SST variability on intraseasonal timescales in the equatorial Pacific Ocean. Many studies have been published on this topic, particularly in the western Pacific where interest in mixed layer processes was stimulated by the Tropical Ocean Global Atmosphere Comprehensive Ocean–Atmosphere Response Experiment (TOGA COARE; Webster and Lukas 1992). Most studies in the western Pacific indicate that one-dimensional processes, and in particular air–sea heat fluxes, are of greatest importance in generating intraseasonal SST variations (Weller and Anderson 1996; Cronin and McPhaden 1997; Shinoda and Hendon 1998; Shinoda et al. 1998). Horizontal advection on the other hand tends to be of secondary importance and entrainment is most effective only during periods of strong winds. Fewer studies have examined the mixed layer temperature balance in the eastern and central Pacific on intraseasonal timescales, in part because the problem is more complicated by three-dimensional advective processes that are less amendable to empirical determination. However, Johnson and McPhaden (1993) and Kessler and McPhaden (1995) have pointed out the importance of zonal advection in the mixed layer temperature balance east of the dateline, and more recently Zhang (2001) has tried to relate intraseasonal SST variations in the eastern and central Pacific to Kelvin-wave-mediated vertical processes. Zhang (2001) noted though, that whereas thermocline depth variations associated with Kelvin waves propagate eastward, SST on intraseasonal timescales tends to be more zonally stationary, or may even appear to propagate westward at times. He explained this odd contrast in behavior as due to a complicated mix of processes operating on SST in the eastern and central Pacific, citing preliminary results of the analysis presented in this paper as a personal communication.

The purpose of this study therefore is to document these processes and to describe how they affect the zonal evolution of SST variability on intraseasonal timescales along the equator. We will use data primarily from the Tropical Atmosphere Ocean (TAO) array of moored buoys focusing on four equatorial sites with long time series. These sites are located in the western Pacific warm pool (165°E), the eastern Pacific equatorial cold tongue (110° and 140°W), and the transition zone between these two regions (170°W). Lack of key datasets limits our analysis to only four sites, but these sites are in regions of great significance for climate, and allow for a consistent comparison of variability in different climatological regimes. A similar analysis examining the mean seasonal cycle and interannual variations in mixed layer temperature along the equator in the Pacific appear in Wang and McPhaden (1999, 2000, 2001a).

The remainder of this paper is organized as follows. In section 2, the datasets, diagnostic equation, and data processing procedures are discussed. Relevant aspects of oceanic and atmospheric variability in the equatorial Pacific on intraseasonal timescales are described in section 3. Section 4 discusses the mixed layer temperature balance at the four buoy locations, and section 5 describes these results in terms of the observed zonal variations in SST. Section 6 provides a discussion and summary of major conclusions.

2. Datasets and processing

a. Datasets

The principal datasets used in this study are from the TAO array (McPhaden et al. 1998), which was implemented as part of the TOGA program to monitor, understand, and predict seasonal-to-interannual climate variability. The array presently consists of approximately 70 deep ocean moorings with 2°–3° meridional spacing and 10°–15° longitudinal spacing, situated between 8°S and 8°N, 137°E and 95°W. Sites are occupied by Autonomous Temperature Line Acquisition System (ATLAS) moorings that measure surface winds, relative humidity, air temperature, SST (nominally at 1-m depth), and temperatures at 10 subsurface depths down to 500 m (Hayes et al. 1991). In addition, along the equator, the array includes several current meter moorings that measure the standard ATLAS variables plus zonal and meridional currents down to the depths of 250–300 m. These currents are measured from either mechanical current meters or acoustic Doppler current profilers (ADCPs), or both. For this study, we also make use of incoming solar radiation measured routinely on

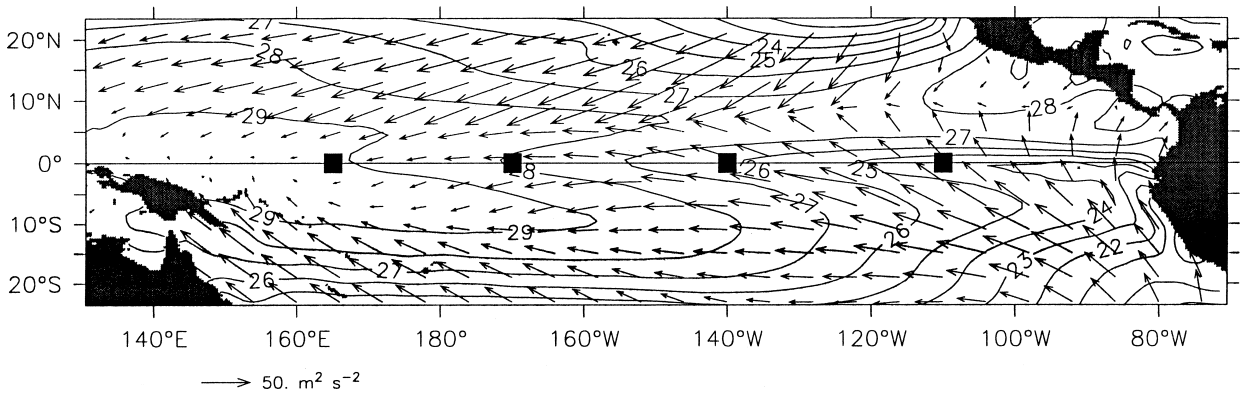

FIG. 1. Mean SST (°C) based on Reynolds and Smith (1994) and mean wind pseudostress ($m^2\ s^{-2}$) based on Goldenberg and O'Brien (1981) in the tropical Pacific. Squares indicate locations of the TAO current mooring measurements used in this study.

the 110°W, 140°W, and 165°E current meter moorings, and salinity measured at 0°, 165°E.

We focus on data from the equatorial current meter moorings (Fig. 1) to estimate terms in the mixed layer temperature balance. The data used at each of these four sites extends through late 1999 and begins (for winds, temperatures, and currents) in 1980 (110°W), 1983 (140°W), 1988 (170°W), and 1986 (165°E). Salinity data are available at 165°E beginning in 1988 (Sprintall and McPhaden 1994). Details of the vertical arrays for temperature and velocity at each site are described Yu and McPhaden (1999). Daily averaged surface heat fluxes at these sites have been computed using a combination of TAO data and outgoing longwave radiation data as outlined below and described in detail in Wang and McPhaden (2001a,b). These heat flux time series begin in 1991 and extend through 1999.

In addition to TAO data, we make use of the Reynolds and Smith (1994) blended satellite/in situ SST analysis. This weekly averaged global product is available on a 1° lat by 1° lon grid from 1982 to 1999. We take advantage of this gridded product, hereafter referred to as ''Reynolds SST,'' for calculating horizontal derivatives of SST. Differences between Reynolds SSTs and collocated TAO SSTs are small enough to be ignored for our purposes (Wang and McPhaden 1999), so that there are no significant inconsistencies in using two different representations of surface temperature in this study.

b. Temperature balance formalism

To understand the roles of various mechanisms in controlling intraseasonal SST variability, we analyze the temperature balance of the upper equatorial Pacific Ocean using a formalism similar to that described in Wang and McPhaden (1999, 2000, 2001a). The mixed layer temperature balance equation can be written as

$$T_t + UT_x + VT_y + \frac{H(W)W\Delta T}{H} = \frac{(Q_0 + Q_{\text{pen}} + Q_H)}{\rho_0 C_p H}, \quad (1)$$

where ρ_0 is seawater density, C_p is heat capacity, H is mixed layer depth, and T is mixed layer temperature. In this equation, T_t represents time rate of mixed layer temperature change; UT_x and VT_y represent zonal and meridional advection, respectively; and $H(W)\ W\Delta T/H$ represents vertical advection and entrainment. The net surface heat flux across the air–sea interface is Q_0. Heat loss by shortwave radiation penetrating below the mixed layer is designated Q_{pen}. Turbulent diffusive heat flux out the base of the mixed layer is designated by Q_H. Positive heat fluxes indicate a gain of heat to the mixed layer.

Mixed layer velocity is denoted by U and V in the zonal and meridional directions, respectively. Here W is the vertical velocity at the base of the mixed layer, and ΔT is the difference between the mixed layer temperature and the temperature of water entrained into the mixed layer. The Heaviside step function $H(W)$ is zero for $W < 0$ and 1 for $W > 0$ in recognition of the fact that entrainment can cool the surface layer but detrainment cannot warm it.

The mixed layer depth is defined as the depth at which the temperature is 0.5°C less than the SST at 170°W, 140°W, and 110°W. At 165°E, variable H was estimated by a density (σ_t) criterion because the importance of salinity in affecting near-surface stratification in the western Pacific. Specifically, H at 165°E is defined as the depth at which $\sigma_t(z = -H) = \sigma_t(z = 0) + (\partial\sigma_t/\partial T)\delta T$ where $\sigma_t = \rho - 1000$ kg m^{-3} and δT is set to 0.5°C (Sprintall and Tomczak 1992). In the absence of salinity variations, this criterion for H reduces to the same as that used at 170°, 140°, and 110°W (Wang and McPhaden 1999). Mean mixed layer depths by these definitions are 59 m (165°E), 71 m (170°W), 45 m (140°W), and 21 m (110°W).

Time rate of temperature change T_t is calculated from TAO temperature data averaged over the mixed layer depth. Zonal advection (UT_x) and meridional advection (VT_y) are computed from TAO velocity data in combination with temperature gradient estimates from Reynolds SST. For zonal advection, T_x is estimated using

centered differences over 4° of longitude, though the calculation was relatively insensitive to SST differencing over distances of 4°–10° of longitude (Wang and McPhaden 2001a). Likewise, we compute meridional advection by estimating T_y from centered differences over 2°N and 2°S.

Mixed layer velocities are gappy at 110°W, 140°W, and 165°E because of data losses from mechanical current meters in the upper 50 m. Thus, we estimate mixed layer velocity from records at 10-m depth, which were much more continuous at these sites. Variations in 10-m and mixed layer velocities are of the same magnitude and highly cross-correlated (ranging between 0.88 and 0.99). Velocities at 10 m are generally more westward on average by several cm s^{-1} compared to mixed layer velocities because of vertical shears between the South Equatorial Current and Equatorial Undercurrent. These mean differences though have little discernable impact in our conclusions. Thus, while using either 10-m or mixed layer velocities in our calculations yields very similar results, we present analyses based on 10-m velocities for which statistical inferences are more robust.

We estimate the vertical velocity as $W = \overline{W} + W'$, where the overbar represents time mean and the prime represents time variations around the mean. This latter quantity is approximated as the difference between time variations in the 20°C isotherm depth and time variations in mixed layer depth, that is, $W' = -\partial h_{20C}/\partial t + \partial H/\partial t$. Accounting for changes in mixed layer depth in the expression for W' eliminates effects due to adiabatic internal wave motions that have no direct effect on mixed layer temperatures (Stevenson and Niiler 1983). It is assumed for this calculation that the 20°C isotherm represents a material surface unaffected by diabatic processes on intraseasonal timescales, and that lateral advection is of secondary importance in determining the temporal variability of either H or h_{20C}. While neither of these assumptions is strictly valid, similar approximations have been used in other tropical ocean mixed layer heat balance studies with reasonable success (e.g., McPhaden 1982; Hayes et al. 1991).

The mean vertical velocity $\overline{W}$ is based on estimates from shipboard ADCP measurements collected between 1991 and 1999 on cruises servicing the TAO array (Johnson et al. 2001). The mean vertical velocity at 50-m depth was estimated in Johnson et al. as $\langle\overline{W}\rangle = 1.9(\pm 0.9) \times 10^{-5}$ m s^{-1}, where the brackets indicate a zonal average between 95° and 170°W. For this study, it is assumed that the mean vertical velocity locally scales with the local mean wind stress; that is,

$$\overline{W}(x) = \langle\overline{W}\rangle\overline{\tau}_x(x)/\langle\overline{\tau}_x\rangle. \quad (2)$$

This expression, when averaged over 95° to 170°W using TAO wind data, reduces to the same $\langle\overline{W}\rangle$ as in Johnson et al. Specific values of $\overline{W}$ from (3) are 1.6×10^{-5} m s^{-1} (110°W), 2.6×10^{-5} m s^{-1} (140°W), 2.1×10^{-5} m s^{-1} (170°W), and 0.5×10^{-5} m s^{-1} (165°E). We assume these values are representative of the mean vertical velocity at the base of the local mixed layer. Other choices for $\overline{W}$ such as obtained by interpolating (at 110° and 140°W) and extrapolating (at 170°W and 165°E) 50-m values to the mean depth of the mixed layer, or by changing 50-m mean values by ±50% [consistent with the level of uncertainty in the Johnson et al. (2001) estimates] do not fundamentally alter our conclusions about the relative importance of processes affecting mixed layer temperature balance.

Following Hayes et al. (1991) and Chang (1993), we assume that entrained water is brought up from approximately 20 m below the mixed layer; that is, $\Delta T = T - T_{H+20m}$. The specification of ΔT was originally rationalized for the eastern equatorial Pacific where salinity was not a factor in determining mixed layer depth. However, it also appropriate at 165°E where the barrier layer is about 20 m thick on average (Zhang and McPhaden 2000). Consistent with previous temperature balance studies in the warm pool, the above specification of ΔT leads to a situation where entrainment fluxes are most pronounced only during those periods of strong westerly winds when the barrier layer is significantly eroded. Other reasonable choices of ΔT do not qualitatively affect our basic conclusions.

Net surface heat flux (Q_0) is estimated as

$$Q_0 = (1 - \alpha)Q_{\text{short}} + Q_{\text{long}} + Q_{\text{latent}} + Q_{\text{sensible}}, \quad (3)$$

where α is the albedo, Q_{short} is incoming shortwave radiation, Q_{long} is net outgoing longwave radiation, Q_{latent} is latent heat flux, and Q_{sensible} is sensible heat flux. A constant albedo value of 0.06 is used based on Payne (1972). Daily values of Q_{short} are based largely on direct hourly measurements from the Eppley radiometers mounted 3.5 m above the sea level on the TAO buoys. To reduce missing data due to gaps in directly measured shortwave radiation, we also constructed daily time series of solar radiation based on Reed's (1977) bulk formula and cloudiness estimates from outgoing longwave radiation (Wang and McPhaden 2001b). Daily values of Q_{long} are estimated using the Clark et al. (1974) bulk formula. Daily averages of Q_{latent} and Q_{sensible} are computed using daily (and, when available, hourly) bulk variables in the Fairall et al. (1996) COARE algorithm. Details of these flux computations and associated error estimates can be found in Wang and McPhaden (2001b).

Penetrative radiation, $Q_{\text{pen}} = -0.45\, Q_{\text{short}} \exp(-\gamma H)$, is calculated using solar radiation and mixed layer depth, assuming an extinction coefficient for sunlight in tropical waters of $\gamma = 0.04$ (equivalent to 25 m). The combination of Q_0 plus Q_{pen} represents the net surface heat flux absorbed by the mixed layer. For simplicity, we will refer this combination as the "adjusted net surface heat flux," Q_{adj}.

Vertical turbulent diffusive flux Q_H can be expressed as $-K\partial T_H/\partial z$ where K is a vertical diffusivity and $\partial T_H/\partial z$ is the vertical temperature gradient at the base of the mixed layer. This term is not explicitly considered because of uncertainties in estimating K with our datasets.

Instead, Q_H will be incorporated into the residual of the regression model for (1) as described in section 4.

c. Data processing and filtering

All individual daily time series (e.g., *T, U, V, W*, etc.) were first averaged on a weekly basis for consistency with the Reynolds SST. Terms in the surface-layer temperature balance (T_t, UT_x, VT_y, $H(W)W\Delta T/H$, $Q_{\text{adj}}/\rho_0 C_p H$) were then computed from these weekly averages. Mean seasonal cycles were calculated and subtracted from each term. The resulting weekly anomalies were low-pass filtered first with a 3-week running mean filter, then a second time series was generated by low passing the data with an 11-week running mean filter. The two versions of low-pass-filtered time series were differenced from one another, creating a bandpassed time series with energy concentrated in the intraseasonal band. The spectral transfer function for this filter has half power at periods of 46 days and 168 days. Application of this filter to the SST time series leads to a variance-weighted frequency of 68 days at 165°E and 170°W, and 69 days at 140° and 110°W. (Variance-weighted frequency is defined as $\hat{f} = \int fS(f)\,df/[\int S(f)\,df]$ where f is frequency and $S(f)$ is spectral density.) Variants of this filtering scheme do not lead to fundamentally different conclusions provided that intraseasonal energy at periods of 50–125 days is sufficiently well represented in the bandpassed time series.

The choice of bandpass filter used in this study reduces variance at periods between 20–40 days where their may be significant intraseasonal energy, particularly in atmospheric variables. This reduction is in part a by-product of the need to filter noise near the Nyquist frequency, which is set by the weekly averaged Reynolds SST. However, emphasis on the lower frequency portion of the intraseasonal band is consistent with the fact that the ocean tends to dynamically filter out the higher-frequency components of intraseasonal wind forcing, naturally shifting the oceanic response spectrum toward lower frequencies (McPhaden and Taft 1988; Kessler et al. 1995; Hendon et al. 1998).

Examples of bandpassed time series at 140°W (Fig. 2) illustrate the magnitudes of intraseasonal variations at this location. Note in particular the close correspondence between SST and mixed layer temperatures based on TAO data. For the purposes of this analysis, we can consider these two quantities as largely interchangeable.

3. Description of temporal/spatial variability

We first describe some of the characteristics of intraseasonal variability along the equator from a basin-scale perspective as a prologue to describing the mixed layer temperature balance in the following section. Time–longitude plots of bandpassed 20°C isotherm depth (a commonly used index for thermocline depth along the equator) for the period 1991–99 show alternating bands of zonally coherent 20°C anomalies along the equator on intraseasonal timescales (Fig. 3). The phase of these 20°C depth variations propagates eastward on average at about 2.2 m s^{-1}, as would be expected for first baroclinic mode Kelvin waves. The maximum standard deviation in 20°C isotherm depth occurs around 140°W (Fig. 4c) because Kelvin wave amplitudes are governed by zonal wind stress integrated along wave characteristics, and the strongest intraseasonal wind forcing lies to the west of 140°W (Fig. 3). Falloff in the amplitude of 20°C depth variations east of 140°W is mirrored by a similar falloff in surface dynamic height variations (Kutsuwada and McPhaden 2002) most likely due to the effects of an eastward shoaling mean thermocline (Fig. 4) on first baroclinic mode Kelvin waves (Giese and Harrison 1990).

The eastern Pacific is where the thermocline is on average shallowest and SST is coldest (Fig. 4), indicating the influence of equatorial upwelling on the mean thermal structure. Largest intraseasonal SST signals are also found in the eastern Pacific, and we expect that these variations may likewise be due at least in part to upwelling processes. Despite relatively weak local zonal wind stress variations in the region (Figs. 3a and 4a), remotely wind-forced equatorial Kelvin waves can affect SST by elevating or depressing the thermocline, making it easier or harder to entrain cold water into the mixed layer. Changes in thermocline depth also lead to changes in near-surface stratification (e.g., Zhang 2001) so that SST can be affected by the temperature of water advected upward by the mean circulation. It is evident from Fig. 3, however, that Kelvin wave–mediated variations in vertical velocity and entrainment cannot be responsible for all the observed SST variations along the equator. Whereas Kelvin waves propagate eastward, intraseasonal variations in SST exhibit little eastward propagation, and at times even propagate westward (e.g., in mid-1998) along the equator.

Lagged correlation analysis of SST and 20°C along the equator (Fig. 5) illustrates this distinction in the behavior of these two quantities quite clearly. In contrast to the approximate 2.2 m s^{-1} eastward phase speed for the 20°C, isotherm depth phase varies little along the equator for SST, and even appears to propagate westward in the eastern Pacific. The tendency for westward propagation was also noted by Zhang (2001). Another interesting feature of the SST correlation pattern is the tendency for SSTs to develop out-of-phase east and west of the international date line, with extrema in the west leading by about 1 week. This tendency for out-of-phase anomaly development is evident in the shift from positive to negative cross-correlation values around 4000 km to the west of 140°W near zero lags (Fig. 5b). Interpretation of these SST features in terms of mixed layer dynamics is the subject of the following two sections.

4. Mixed layer heat balance

In this section we diagnose a linear least squares regression model of mixed layer temperature change formulated as

$$T_t = \beta_1 \frac{Q_{\text{adj}}}{\rho_0 C_p H} - \beta_2 \frac{H(W)W\Delta T}{H} - \beta_3 UT_x - \beta_4 VT_y + \epsilon, \quad (4)$$

where the β_n are regression coefficients and ϵ is residual variability. The residuals contain sampling, computational, and instrumental errors, as well as unresolved physical processes such as vertical turbulent diffusion. We first solve (4) for each term individually to highlight individual processes, then for all four terms simultaneously. Standard deviation (σ), cross correlation (R), and regression coefficient (β) are used as a guide to help assess the relative importance of the terms individually. Terms are considered to be of increasing importance as their standard deviations approach that of T_t, and as cross correlations and regression coefficients approach unity.

All available data are used for term-by-term regression analysis in (4). Differences in data gaps for terms on the right side of (4) mean that record lengths and periods covered in the analysis of individual terms will be different. However, the records are long enough and the statistics are stationary enough that these differences do not significantly affect the results. For the multiple linear regression analysis described in section 4e and summarized in Table 1, record lengths for all the terms are identical.

a. Surface heat flux

As described in previous studies (e.g., Kessler and McPhaden 1995; Weller and Anderson 1996; Cronin and McPhaden 1997; Shinoda et al. 1998) intraseasonal variations in Q_0 are primarily due to variations in Q_{short} and Q_{latent}, with Q_{long} and Q_{sensible} of secondary importance. Intraseasonal standard deviations in Q_{short} and Q_{latent}, range between 7–11 W m^{-2} and 10–16 W m^{-2}, respectively, with highest values at 165°E and lowest at 110°W. Likewise, the highest intraseasonal variability in total surface heat flux Q_0 occurs at 165°W (27 W m^{-2}) and the lowest at 110°W (13 W m^{-2}). Intraseasonal variations in the penetrative component of radiation Q_{pert} are largest and most important at 110°W (standard deviation of 3.2 W m^{-2}) where the mixed layer is relatively shallow.

Surface heat flux adjusted for penetrative radiation is increasingly important as a cause of mixed layer temperature variability as one progresses westward along the equator (Fig. 6). At 165°E, the standard deviation of $Q_{\text{adj}}/\rho_0 C_p H$ is nearly identical to that of T_t, the cross correlation is over 0.7 and highly statistically significant, and β is close to unity. Cross correlation and regression coefficients decrease eastward, and are not significantly different from zero at 140° and 110°W. Large variations in $Q_{\text{adj}}/\rho_0 C_p H$ at 110°W result from surface heat fluxes being stored in a relatively shallow mixed layer in the equatorial cold tongue region. However, by themselves these large variations are not a measure of the importance of surface heat fluxes in generating intraseasonal SST variations in the eastern Pacific.

Another perspective on the role of local surface fluxes can be found by regressing Q_0 onto mixed layer temperature rather than T_t (Fig. 7). The cross correlation between these two quantities is indistinguishable from zero in the west, but progressively becomes more negative and statistically significant toward the east. The sign of the regression implies that surface fluxes act as a negative feedback on intraseasonal SST variations in much the same way as occurs on seasonal-to-interannual timescales in the eastern Pacific (Wang and McPhaden 1999, 2000, 2001a). In magnitude, negative feedbacks associated with turbulent heat fluxes are larger and more significant than those associated with cloud–radiative feedbacks. However, both act to cool the surface when SSTs are elevated and to warm the surface when SSTs are depressed. The regression coefficient implies damping at a rate of about 20 W m^{-2} °C^{-1} between 110° and 170°W for intraseasonal mixed layer temperature variations. For mixed layer depths of 20–60 m, this leads to damping timescales of about 1.5–4.5 months. These damping times are about 4–10 times longer than the 11-day timescale of intraseasonal bandpassed mixed layer temperature variations estimated from $2\pi\hat{f}^{-1}$, where $\hat{f}$ is variance weighted frequency.

Thus, our results are consistent with previous analyses that indicate a central role for local surface heat fluxes in generating intraseasonal SST variations in the western Pacific warm pool, and with a hypothesis that surface fluxes act to damp intraseasonal SST variations generated by ocean dynamical processes in the eastern and central Pacific. The effects of these dynamical processes on the mixed layer temperature balance are described in the following three subsections.

b. Vertical advection and entrainment

Vertical advection and entrainment, $H(W)W\Delta T/H$, has a significant effect on intraseasonal mixed layer temperature variations, especially in the eastern Pacific (Fig. 8). The amplitude of this term, and its cross correlation with T_t, are largest at 110°W. Cross correlation is also highly significant at 140°W, and regression coefficients at 110° and 140°W are close to unity.

The term $H(W)W\Delta T/H$ is likewise highly correlated with T_t, and the regression coefficient is close to unity, at 165°E. This implies that vertical heat fluxes are important at this location, even though their standard deviation is two to four times smaller than in the eastern Pacific. The lowest correlation between T_t and $H(W)W\Delta T/H$, and the smallest regression coefficient, are found at 170°W. The mixed layer is deepest on average at this longitude, so it could be that the effects of vertical advection and entrainment on mixed layer tem-

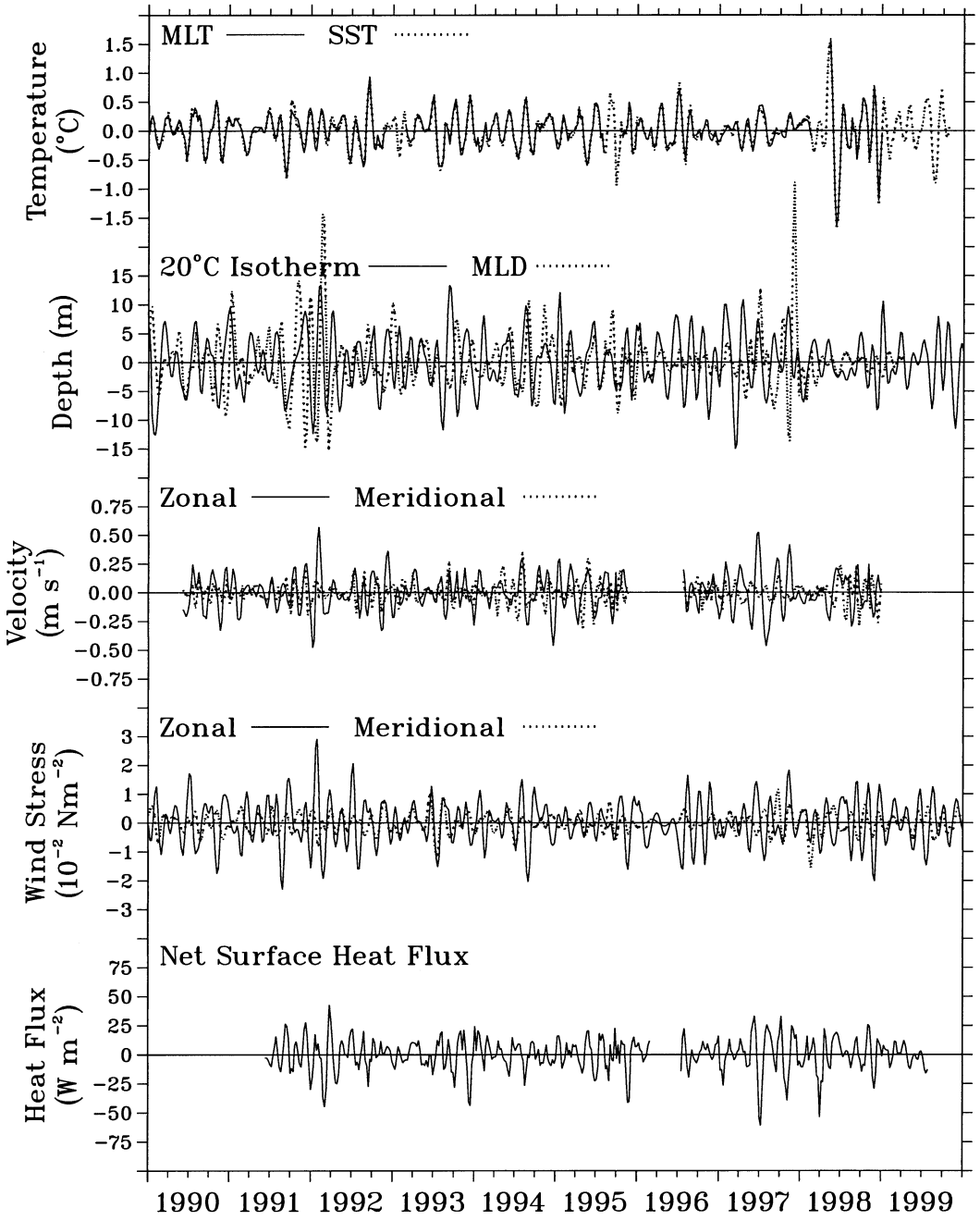

FIG. 2. Time series of intraseasonal SST, mixed layer temperature (MLT), mixed layer depth (MLD), 20°C isotherm depth, zonal and meridional currents at 10-m depth, zonal and meridional surface wind stress, and net surface heat flux (Q_0) at 0°, 140°W. Wind stress is computed from daily data using a constant air density of 1.2 kg m^{-3} and a drag coefficient of 1.2×10^{-2}. Surface heat flux is computed as described in section 2b. Positive (negative) 20°C isotherm and mixed layer depths imply deeper (shallower) levels.

perature are diluted relative to locations farther east and west.

We repeated these calculations for different versions of the vertical advection and entrainment term in order to identify the processes that give rise to its variations. For two of these versions, we used $H(W)\overline{W}\Delta T''$ and $H(W)W''\overline{\Delta T}$, where overbar indicates time mean and the double prime indicates bandpassed intraseasonal variations. These alternative expressions test the importance of mean advection of the intraseasonally varying temperature field and intraseasonal advection of the mean temperature field, respectively. Results indicate that in general, the term involving variable vertical velocity W'' is more important in the temperature balance

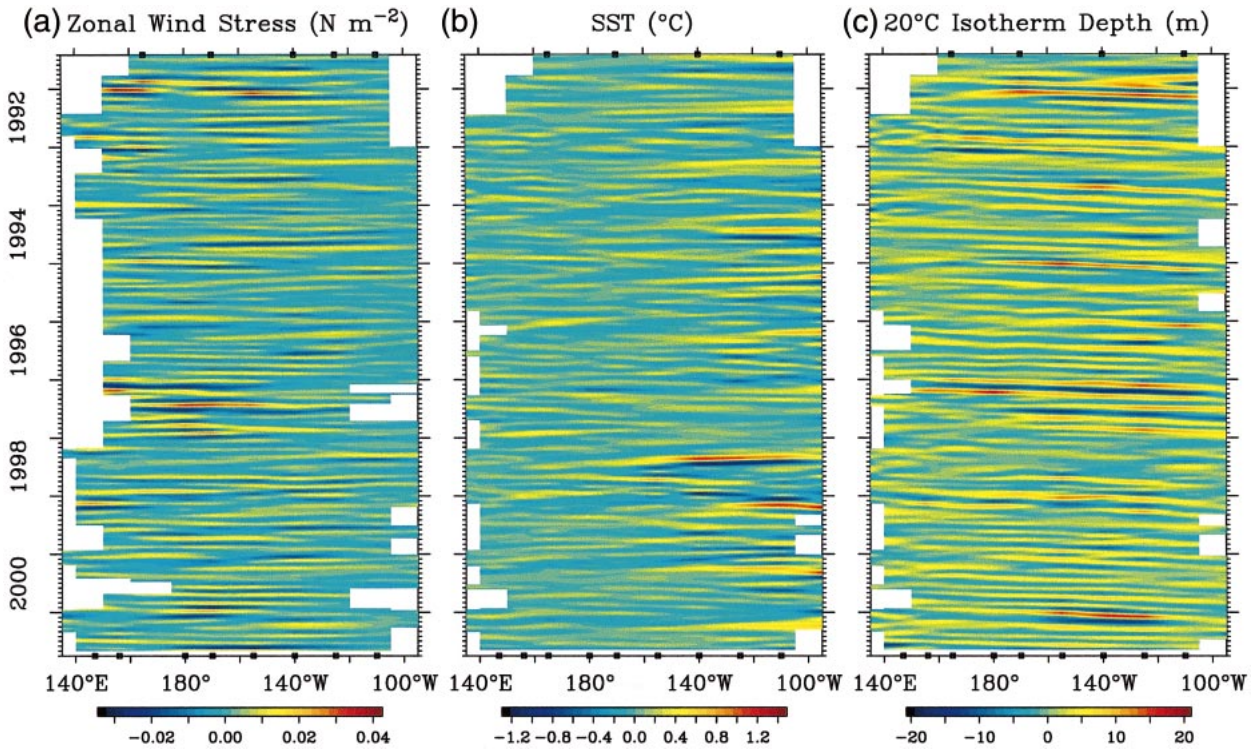

FIG. 3. Time–longitude plots of intraseasonal zonal wind stress (N m^{-2}), SST (°C), and 20°C isotherm depth (m) averaged between 2°N and 2°S along the equator for 1991–99. Squares along the longitudinal axis indicate locations where data were available at the (top) start and (bottom) end of the time series.

than the term involving the mean vertical velocity W, but in the eastern and central Pacific both are significant. Much of the intraseasonal variability associated with W'' and $\Delta T''$ east of the date line is related to remotely forced equatorial Kelvin waves (Fig. 3; Zhang 2001; Kutsuwada and McPhaden 2002). Hence, interaction of these waves with mean background hydrodynamic conditions plays a significant role in affecting mixed layer temperature, particularly at 110° and 140°W.

We also considered a form of $H(W)W\Delta T/H$ that takes into account only nonlinear interactions, by first subtracting mean W and mean ΔT from the weekly vertical velocity and temperature time series (i.e., $W' = W - \overline{W}$, $\Delta T' = \Delta T - \overline{\Delta T}$) and then intraseasonally bandpassing their product. This computation, which includes nonlinear interactions across all resolved timescales (from weekly to interannual), was smaller and of secondary importance compared to $H(W)\overline{W}\Delta T''$ and $H(W)W''\overline{\Delta T}$, except at 140°W. As described below, nonlinear effects in vertical advection and entrainment at 140°W may result from a modulation of tropical instability wave activity on intraseasonal timescales at this site.

Another version of $H(W)W\Delta T/H$ was examined in which the term $\partial H/\partial t$ in W was set to zero. This version tests the relative importance of local mixed layer turbulent processes vis-a-vis large-scale ocean dynamical processes (which govern W and $\partial h_{20C}/\partial t$) in affecting entrainment fluxes. When $\partial H/\partial t$ is set to zero, the most significant change occurs at 165°E where the cross correlation with T_t drops to statistically insignificant near-zero levels (Fig. 9). Other locations are also affected, but not to the extent that the results at those locations are fundamentally altered. Thus, we conclude that in the western Pacific warm pool, entrainment fluxes are mediated mainly by mixed layer turbulence, whereas east of the date line ocean dynamical processes, primarily those associated with intraseasonal equatorial Kelvin waves, are essential.

c. Zonal advection

Zonal advection is generally significant at all longitudes, though only marginally so at 110°W (Fig. 10). Also, while the magnitude of zonal advection is roughly constant in an absolute sense across the basin, it decreases relative to the magnitude of T_t east of 170°W. Regression slopes (β) are significantly less than unity, ranging from 0.6 at 165°E, 170°W, and 140°W to 0.3 at 110°W. Based on magnitudes, correlation coefficients, and regression slopes, zonal advection appears to be less important in the mixed layer temperature balance than surface heat flux forcing at 165°E and less important than vertical advection and entrainment at 110° and 140°W. In contrast, zonal advection is relatively more

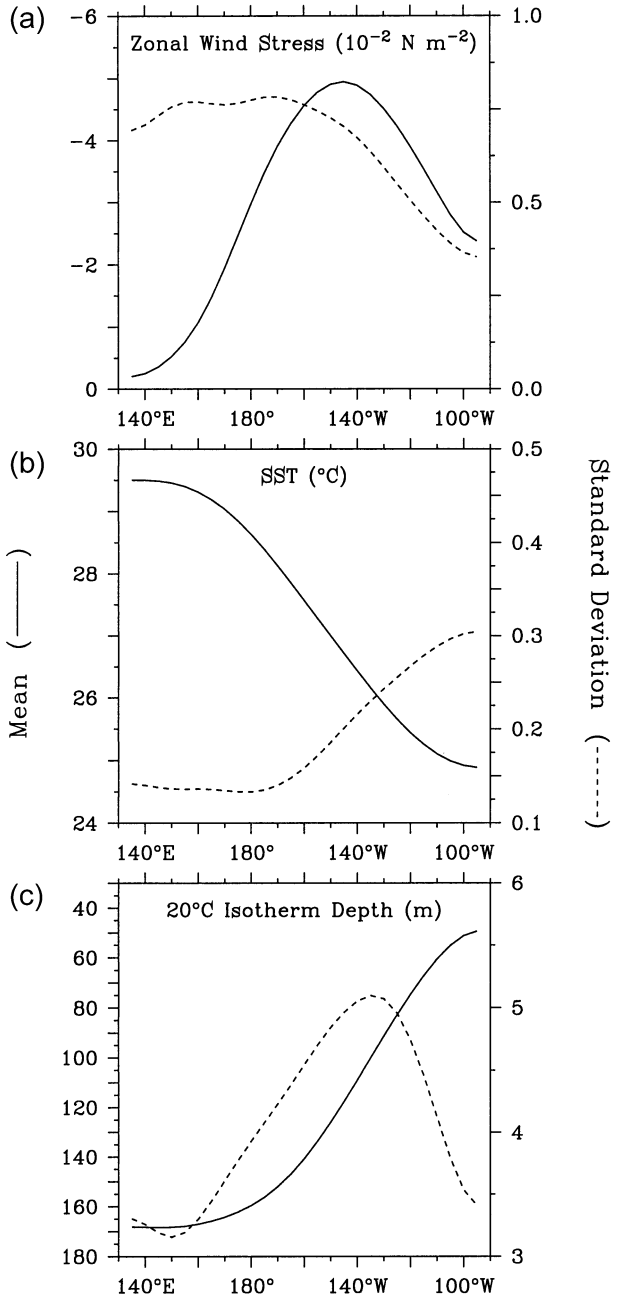

FIG. 4. Record length mean (solid lines and left axes) and standard deviation of intraseasonal timescale variations (dashed lines and right axes) in (a) zonal wind stress (N m^{-2}), (b) SST (°C), and (c) 20°C isotherm depth (m) along the equator for 1991–99.

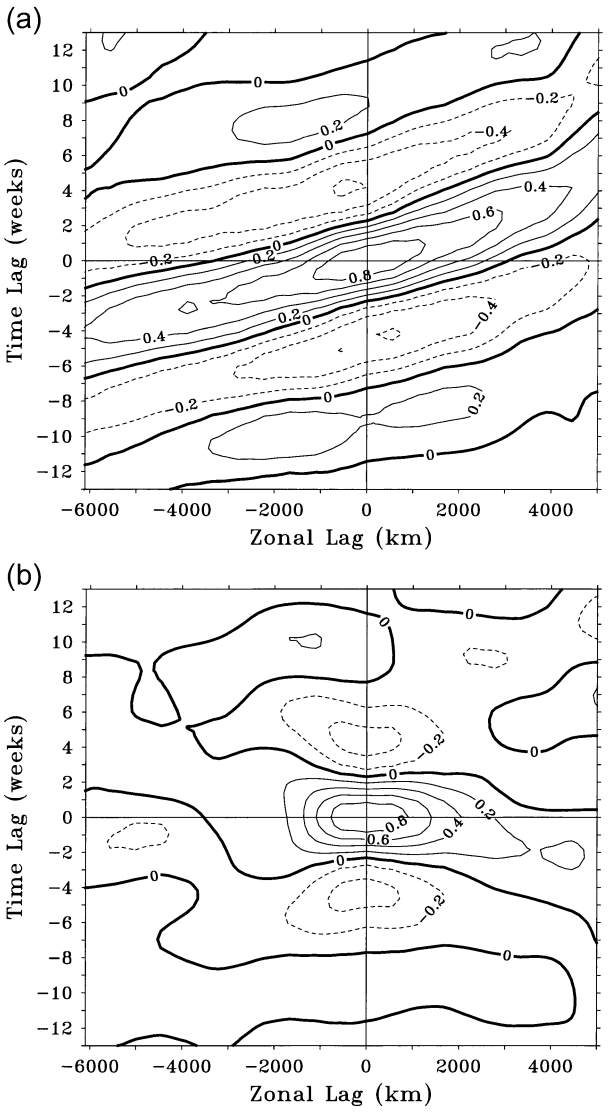

FIG. 5. Lagged correlation along the equator as a function of time and longitude relative to 0°, 140°W for (a) 20°C isotherm depth and (b) SST for the period 1991–99.

prominent at 170°W than at other locations in affecting mixed layer temperature variability.

In an absolute sense, most of the correlation with T_t between 110° and 170°W comes from advection of the mean temperature gradient by intraseasonal currents ($U''\overline{T}_x$) (Fig. 11). Intraseasonal zonal currents (U'') are for the most part directly wind forced in the western Pacific and related to remotely forced Kelvin waves in the eastern Pacific (Kutsuwada and McPhaden 2002). At 170°W, variations in U'' are a combination of these two dynamical effects since there are times during El

TABLE 1. Percent of intraseasonal T_t variance explained by various terms in the temperature balance equation (4) along the equator.

	Zonal advection	Meridional advection	Vertical advection and entrainment	Adjusted surface heat flux
110°W	0.2	1.4	23.0	0.0
140°W	9.5	13.5	11.9	0.6
170°W	16.2	3.5	6.1	3.8
165°E	5.2	0.8	6.8	31.0

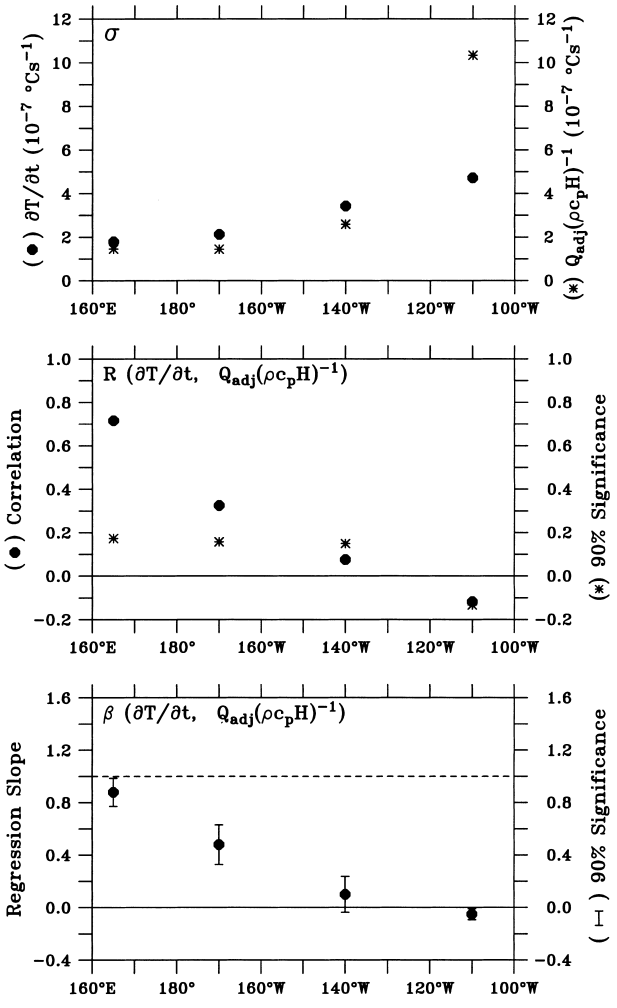

FIG. 6. Results of regression analysis for intraseasonally bandpassed T_t and $Q_{adj}/\rho_0 C_p H$ in terms of (top) standard deviations (σ), (middle) cross correlations (R), and (bottom) regression coefficients (β). $\beta = 1$ is indicated by the dashed line. Ninety percent confidence limits for R and β are also shown.

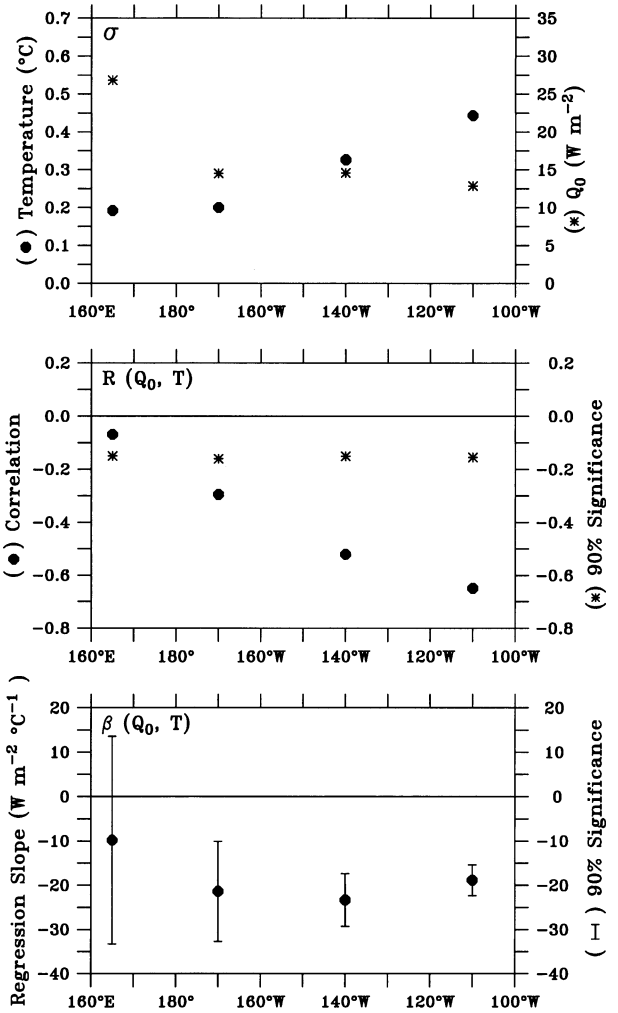

FIG. 7. Results of regression analysis for intraseasonally bandpassed mixed layer temperature T and surface heat flux Q_0 in terms of (top) standard deviations (σ), (middle) cross correlations (R), and (bottom) regression coefficients (β). $\beta = 1$ is indicated by the dashed line. Ninety percent confidence limits for R and β are also shown.

Niño events when direct wind forcing extends east of the date line.

At 165°E, advection of the mean temperature field by intraseasonally varying currents ($U''\overline{T}_x$) is negligible (Fig. 11) because the mean zonal gradient is weak there (Fig. 1). Nonlinear effects (obtained by bandpassing $U'T'_x$, where U' and T'_x are demeaned time series) account for most of intraseasonal zonal advection signal at this location. Nonlinearities are significant, but of lesser importance, at both 170° and 140°W.

d. Meridional advection

In magnitude, VT_y tracks T_t along the equator, with both terms increasing eastward (Fig. 12). However, we can infer that meridional advection is relatively unimportant compared to the dominant terms in the heat balance at 165°E and 170°W. At these locations, VT_y amplitudes are small, correlations with T_t are weak, and regression coefficients are much less than unity. Conversely, correlations are higher and significantly nonzero at 140° and 110°W. Splitting VT_y into various components as for zonal and vertical advection, we find that nonlinear advection (obtained by bandpassing $V'T'_y$, where V' and T'_y are demeaned time series) is the main contribution to meridional advection at 140°W. Tropical instability waves are most energetic between 125° and 140°W (Halpern et al. 1988), and Harrison and Giese (1988) have shown that the passage of wind-forced Kelvin waves in the eastern Pacific can alter the large-scale current shears on which they depend. Thus, as occurs on seasonal and interannual timescales (Philander et al. 1985; Wang and McPhaden 1999, 2000), meridional heat fluxes associated with tropical instability

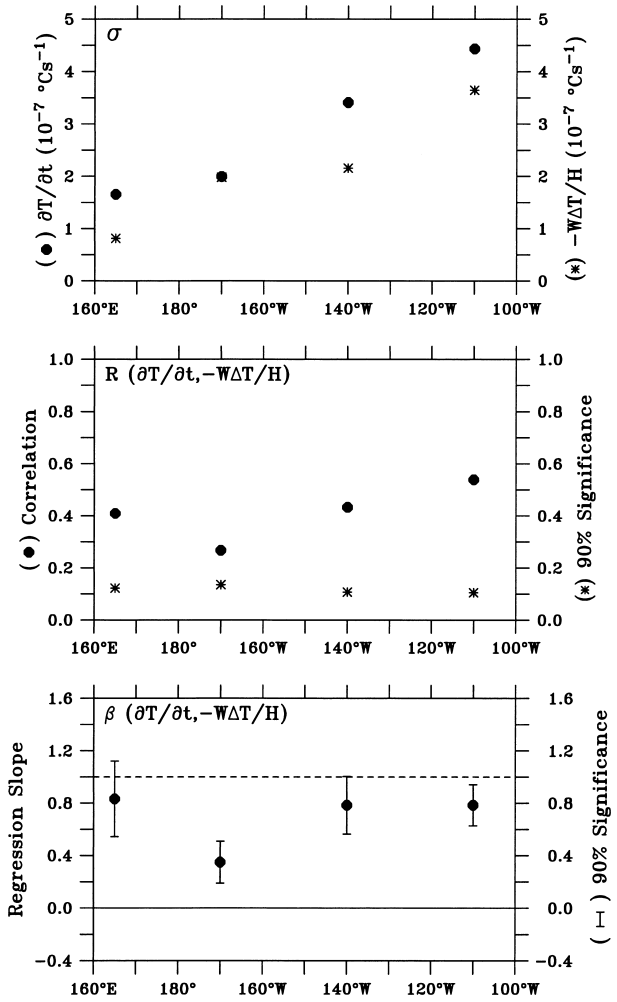

FIG. 8. Results of regression analysis for intraseasonally bandpassed T_t and vertical advection and entrainment [written as $-H(W)W\Delta T/H$ for consistency with (4)] in terms of (top) standard deviations (σ), (middle) cross correlations (R), and (bottom) regression coefficients (β). $\beta = 1$ is indicated by the dashed line. Ninety percent confidence limits for R and β are also shown.

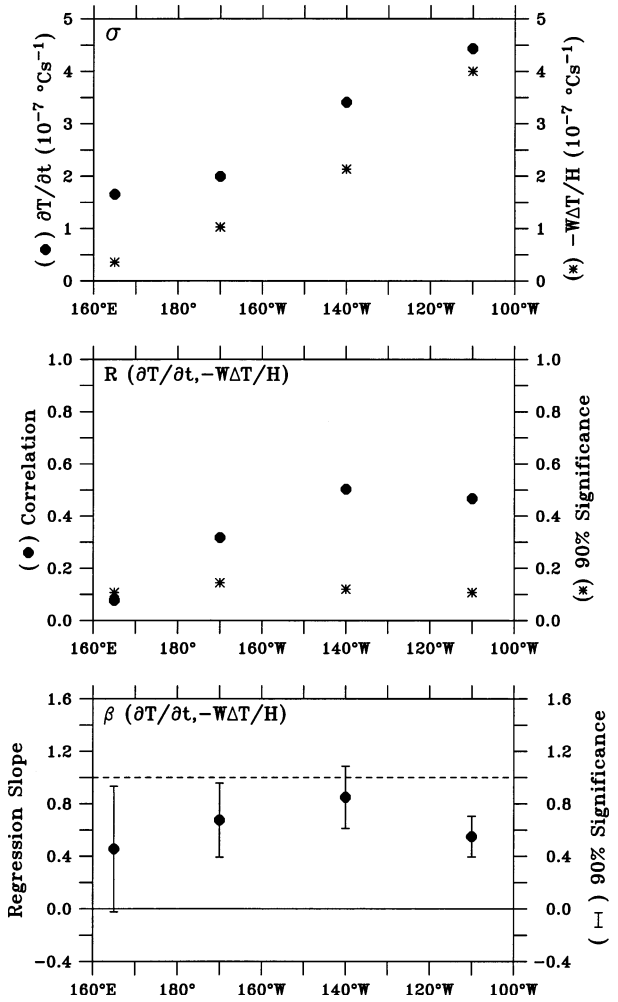

FIG. 9. Results of regression analysis for intraseasonally bandpassed T_t and vertical advection and entrainment [written as $-H(W)W\Delta T/H$ for consistency with (4)] in terms of (top) standard deviations (σ), (middle) cross correlations (R), and (bottom) regression coefficients (β). In this instance, $\partial H/\partial t$ in W is set to zero. $\beta = 1$ is indicated by the dashed line. Ninety percent confidence limits for R and β are also shown.

waves may be modulated on intraseasonal timescales, an effect that could account for the relative importance of VT_y in the surface-layer temperature balance at 140°W (Fig. 12).

Advection of the mean temperature field by intraseasonal timescale meridional velocity variations, $V''\overline{T}_y$, is the principal reason for the importance of meridional advection at 110°W. The mean meridional temperature gradient is relatively large on the equator in the eastern Pacific because the central axis of the cold tongue is centered south of the equator (Fig. 1). Intraseasonal variations in V at this location may arise from the low-frequency portion of the tropical instability wave spectrum; alternately, they may be generated by Kelvin waves interacting with a hemispherically asymmetric background state (McPhaden and Knox 1979; Philander 1979).

e. Multiple linear regression

Solving (4) for all terms simultaneously provides a systematic evaluation of various processes affecting T_t. Consistent with inferences derived from the univariate analyses described above, local surface heat fluxes play a dominant role in the western Pacific (165°E), zonal advection is most prominent in the central Pacific (170°W), and vertical advection and entrainment are largest in the eastern Pacific (110° and 140°W) (Table 1). We note, however, that the percent variance of T_t explained by the sum of terms on the right side of (4)

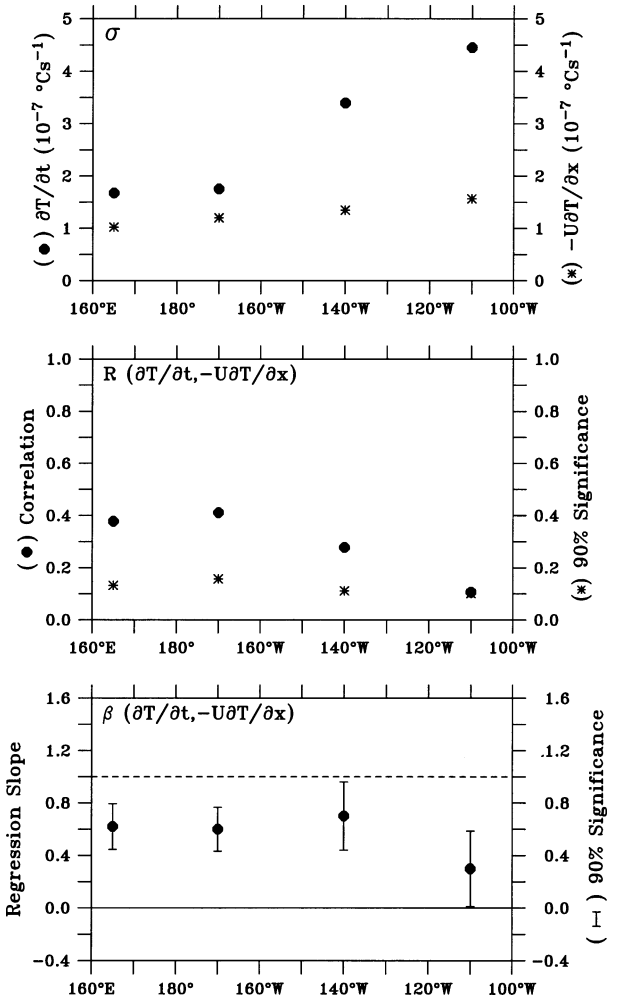

FIG. 10. Results of regression analysis for T_t and zonal advection [written as $-UT_x$ for consistency with (4)] in terms of (top) standard deviations (σ), (middle) cross correlations (R), and (bottom) regression coefficients (β). $\beta = 1$ is indicated by the dashed line. Ninety percent confidence limits for R and β are also shown.

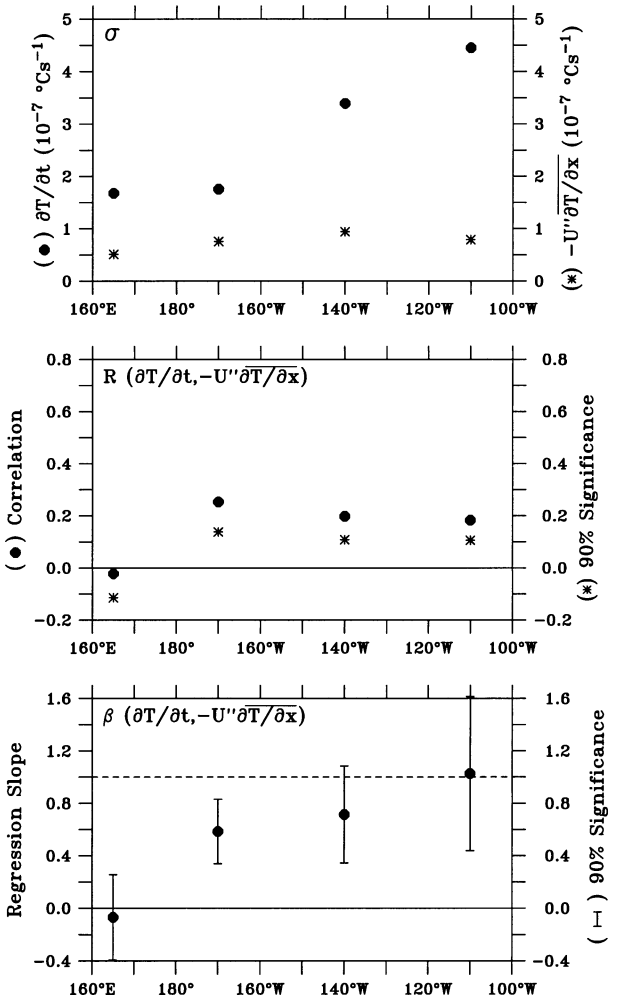

FIG. 11. Results of regression analysis for intraseasonally bandpassed T_t and zonal advection [written as $-UT_x$ for consistency with (4)] in terms of (top) standard deviations (σ), (middle) cross correlations (R), and (bottom) regression coefficients (β). In this instance, zonal advection is represented by just advection of the mean temperature field by intraseasonal zonal velocity variations, i.e., $U''\overline{T}_x$. $\beta = 1$ is indicated by the dashed line. Ninety percent confidence limits for R and β are also shown.

ranges between 24% and 43%, so that there is still a significant part of the variability that we cannot account for. The imperfect fit of our regression equation to observed T_t is no doubt influenced by the approximate nature of our estimates, which are contaminated by sampling, computational, and instrumental errors in varying degrees. In addition, neglected physical processes may also affect the goodness of fit. For example, the decrease in variance explained from 165°E to 110°W may result from a neglect of turbulent diffusive fluxes, Q_H, which one might expect to be larger in the eastern Pacific in association with the vertical shears above the core of the Equatorial Undercurrent. Nonetheless, despite these shortcomings in our empirical approach, we have been able to quantify the relative importance of various terms in the surface-layer temperature balance in physically consistent framework across the equatorial Pacific basin.

5. Discussion

Based on the results of the previous section, we are now in a position to interpret the different behaviors of SST and 20°C depth evident in Fig. 5 and as discussed in Zhang (2001). According to linear theory (Moore and Philander 1977), equatorial Kelvin waves propagate from west to east along the equator. For first baroclinic mode Kelvin waves, which are most prominent in our results, variations in surface zonal velocity and 20°C isotherm depths should be in phase with one another. For a pure Kelvin wave in a resting ocean, SST vari-

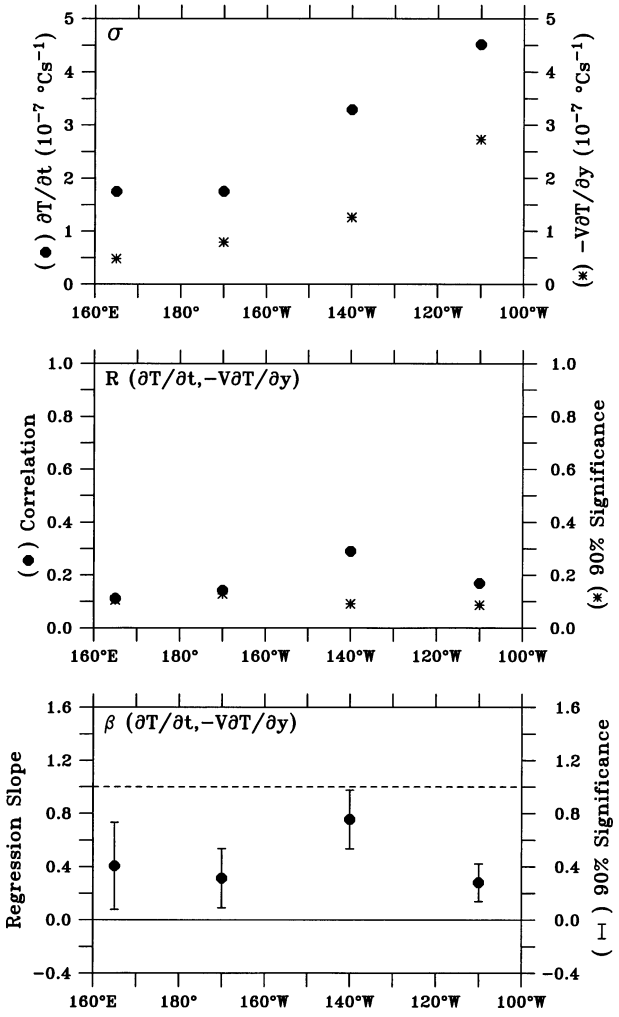

FIG. 12. Results of regression analysis for intraseasonally bandpassed T_t and meridional advection [written as $-VT_y$ for consistency with (4)] in terms of (top) standard deviations (σ), (middle) cross correlations (R), and (bottom) regression coefficients (β). $\beta = 1$ is indicated by the dashed line. Ninety percent confidence limits for R and β are also shown.

ations are zero by definition. However, when the background state is nonuniform, and in particular when there are mean SST gradients, intraseasonal SST variations can be linked to Kelvin wave dynamics in a perturbation sense through mixed layer processes that do not affect the dynamics of the waves themselves.

Now consider a mixed layer temperature balance deliberately simplified to illustrate how Kelvin waves can influence surface temperatures. At 170°W, where zonal advection is the most prominent mechanism controlling mixed layer temperature on intraseasonal timescales, we can write in approximate form $T_t \sim -U''\overline{T}_x$. This expression assumes that all the bandpassed variance in zonal velocity is related to Kelvin wave dynamics, and that other terms in the surface-layer temperature balance are negligible. Under these conditions, mixed layer temperature T would lag Kelvin wave surface zonal velocity (and therefore 20°C depth) by about 1/4 of a cycle. Conversely, in the eastern Pacific, a significant percentage of mixed layer temperature variability is governed by $T_t \sim -H(W)W''\overline{\Delta T}/H$, where $W'' \sim -\partial h_{20C}/\partial t$ represents vertical velocity variations associated with intraseasonal Kelvin waves. In this limit, intraseasonal variations in U, h_{20C} and T are all in phase. Thus, because of the different processes controlling mixed layer temperatures at different locations along the equator, zonal phase variations in intraseasonal Kelvin wave generated surface temperatures will not be the same as those for the Kelvin wave itself.

The exact character of SST phasing across the basin in this simple example depends on the time it takes for a Kelvin wave to transit from the central Pacific to the eastern Pacific (t_K) versus the time it takes for SST to respond to zonal advection in the central Pacific (t_U). In particular, if $t_K \sim t_U$, it is possible for SST variations to appear to develop in phase across the basin. On the other hand, if $t_K < t_U$ (i.e., the time for a Kelvin wave to travel from the central to the eastern Pacific is short relative to the time it takes for SST to respond to zonal advection in the central Pacific), SST may appear to propagate westward. For observed intraseasonal variability, t_K and t_U are both roughly on the order of 15 days to 1 month. Thus, based on this simple example, it is possible to qualitatively explain the very different behaviors in SST and h_{20C} along the equator on intraseasonal timescales.

There are instances when intraseasonal Kelvin waves are not strongly evident, yet there appears to be westward propagation of both warm and cold SST anomalies. Mid-1998 is one such instance (Figs. 2 and 3), when surface winds associated with an unusual episode of MJO forcing extended into the eastern Pacific (Takyabu et al. 1999). In this case, one can invoke a similar set of arguments to account for the observed SST variability, but in terms of local wind forcing rather than remotely wind-forced Kelvin waves. In particular, in a situation where zonal winds strengthen abruptly over a wide range of longitudes as occurred at the end of the 1997/98 El Niño, SST would respond most strongly to local upwelling in the eastern Pacific where the thermocline is shallow, but most strongly to zonal advection in the central Pacific where a deeper mixed layer dilutes the effects of local upwelling. In these circumstances, SST decreases in the eastern Pacific would lead those farther west. By the same logic, westerly winds intensifying simultaneously over a wide range of longitudes would lead to rising SSTs first in the eastern Pacific and later in the central Pacific.

6. Summary and conclusions

In the foregoing sections we have quantified to the extent possible the physical processes involved in generating SST variability on intraseasonal timescales in

the equatorial Pacific. We have found that local surface heat fluxes play a dominant role in the western Pacific (165°E), zonal advection is most prominent in the central Pacific (170°W), and vertical advection and entrainment are largest in the eastern Pacific (110° and 140°W). Remotely forced equatorial Kelvin waves are important in mediating intraseasonal SST variations east of the date line, though local wind forcing can contribute there as well. Surface heat fluxes tend to damp intraseasonal SST variations generated by ocean dynamical processes in the eastern and central Pacific at a rate of about 20 W m^{-2} $°C^{-1}$.

These results provide a framework for interpreting apparent discrepancies in the behavior of intraseasonal SST and 20°C isotherm depth variations in the equatorial Pacific pointed out by Zhang (2001) and apparent in Figs. 3 and 5. They also provide an explanation for the inexplicable SST ''warming and cooling events in the central/eastern Pacific occur[ing] nearly simultaneously over a wide longitude range'' during the onset and decay of the 1991/92 El Niño as noted by Kessler and McPhaden (1995). These SST warming and cooling events occurred very abruptly in association with intraseasonal downwelling and upwelling Kelvin waves, but how precisely they were linked to Kelvin wave processes was left unanswered in that study.

The premise that intraseasonal SST and 20°C isotherm depth variations should propagate eastward at Kelvin wave speeds presumes that mixed layer temperatures are coupled to Kelvin wave dynamics through a single dominant process. However, as we have shown, the processes affecting mixed layer temperature evolve from west to east along the equator. In particular, the combination of Kelvin wave–mediated zonal advection in the central Pacific plus vertical advection and entrainment in the eastern Pacific can plausibly produce SST variations that are nearly in phase across a wide range of longitudes, or even appear to propagate westward in certain instances.

The degree to which intraseasonal atmospheric wind forcing can influence the lower frequency evolution of year-to-year climate variations associated with the ENSO cycle may in part depend on the zonal extent of the induced intraseasonal SST variations. Kessler et al. (1995), for example, argued for the importance of intraseasonal SST variations caused by zonal advection of the eastern edge of the warm pool during the onset of El Niño, whereas Zhang (2001) argued for the importance of SST variations caused by vertical advection associated with Kelvin waves. As we have shown in this study, both of these processes can potentially work together to produce nearly simultaneous warming of equatorial SSTs over several thousands of kilometers. At the same time, the westerly winds that cause warming east of the date line are associated with surface cooling in the western Pacific (Fig. 5b) primarily through enhanced latent heat fluxes and reduced insolation. The broad zonal extent of warm SSTs east of the date line, coupled with cooling in the warm pool, could facilitate the eastward migration of deep convection and so contribute to the initiation of El Niño events (Kessler and Kleeman 2000). Similarly, during the termination phase of El Niño, the sudden and simultaneous development of cold SSTs along the equator east of the date line could rapidly shut down deep convection over a wide range of longitudes, and so nudge the system toward La Niña conditions.

These arguments are not meant to imply that intraseasonal atmospheric forcing is a sufficient condition of the initiation of El Niño or La Niña events. However, if large-scale conditions are favorable, intraseasonal SST changes and their feedbacks to the atmosphere can influence the development of interannual variability (e.g., Kirtman and Schopf 1998; Moore and Kleeman 1999; Bergman et al. 2001). Thus, since intraseasonal timescale fluctuations represent a form of stochastic forcing on the climate system, they can contribute to the observed irregularity of the ENSO cycle in terms of amplitude, duration, frequency, and the detailed evolution of individual events. In addition, the predictability of intraseasonal weather variability is limited by nonlinear chaos to only about 2 weeks (e.g., Waliser et al. 1999b; Hendon et al. 2000). Therefore, to the extent that intraseasonal variations can affect the details of ENSO variability, they can also affect the predictability of that variability.

The results described in this study are based on limited datasets at only a few locations. Moreover, the analysis is limited by various sources of noise, and by the inability to resolve all relevant physical processes. Thus, it would be valuable to examine the issues raised in this paper in the context of dynamical wind-forced ocean models and (if possible) coupled ocean atmosphere models. Conclusions about which terms are important in the surface-layer heat balance as a function of longitude, and how large-scale intraseasonal SST anomalies affect the atmosphere, should be immanently testable within the framework of dynamical numerical models that produce realistic forms of intraseasonal variability.

Acknowledgments. Billy Kessler of NOAA/Pacific Marine Environmental Laboratory (PMEL) and Chidong Zhang of the University of Miami are gratefully acknowledged for helpful comments on this manuscript. Special thanks to Margie McCarty of NOAA/PMEL and the Joint Institute for the Study of the Atmosphere and Ocean (JISAO) at the University of Washington for assistance with computations and graphics. This work was supported by NOAA's Office of Oceanic and Atmospheric Research and by JISAO under NOAA Cooperative Agreement NA17RJ1232.

REFERENCES

Bergman, J. W., H. H. Hendon, and K. M. Weickmann, 2001: Intraseasonal air–sea interactions at the onset of El Niño. *J. Climate,* **14,** 1702–1719.

Chang, P., 1993: Seasonal cycle of sea surface temperature and mixed layer heat budget in the tropical Pacific Ocean. *Geophys. Res. Lett.,* **20,** 2079–2082.

Clark, N. E., L. Eber, R. M. Laurs, J. A. Renner, and J. F. T. Saur, 1974: Heat exchange between ocean and atmosphere in the eastern North Pacific for 1961–71. NOAA Tech. Rep. NMFS SSRF-682.

Cronin, M. F., and M. J. McPhaden, 1997: The upper ocean heat balance in the western equatorial Pacific warm pool during September–December 1992. *J. Geophys. Res.,* **102,** 8533–8553.

Fairall, C. W., E. F. Bradley, D. P. Rogers, J. B. Edson, and G. S. Young, 1996: Bulk parameterization of air–sea fluxes for Tropical Ocean Global Atmosphere Coupled Ocean–Atmosphere Response Experiment algorithm. *J. Geophys. Res.,* **101,** 3747–3764.

Flatau, M., P. J. Flatau, P. Phoebus, and P. P. Niiler, 1997: The feedback between equatorial convection and local radiative and evaporative processes: The implications for intraseasonal oscillations. *J. Atmos. Sci.,* **54,** 2373–2386.

Giese, B. S., and D. E. Harrison, 1990: Aspects of the Kelvin wave response to episodic wind forcing. *J. Geophys. Res.,* **95,** 7289–7312.

Goldenberg, S. B., and J. J. O'Brien, 1981: Time and space variability of tropical Pacific wind stress. *Mon. Wea. Rev.,* **109,** 1190–1207.

Halpern, D., R. A. Knox, and D. S. Luther, 1988: Observations of 20-day period meridional current oscillations in the upper ocean along the Pacific equator. *J. Phys. Oceanogr.,* **18,** 1514–1534.

Harrison, D. E., and P. S. Schopf, 1984: Kelvin wave induced advection and the onset of SST warming in El Niño events. *Mon. Wea. Rev.,* **112,** 923–933.

——, and B. S. Giese, 1988: Remote westerly wind forcing of the eastern equatorial Pacific: Some model results. *Geophys. Res. Lett.,* **15,** 804–807.

Hayes, S. P., L. J. Mangum, J. Picaut, A. Sumi, and K. Takeuchi, 1991: TOGA TAO: A moored array for real-time measurements in the tropical Pacific Ocean. *Bull. Amer. Meteor. Soc.,* **72,** 339–347.

Hendon, H. H., B. Liebmann, and J. D. Glick, 1998: Oceanic Kelvin waves and the Madden–Julian oscillation. *J. Atmos. Sci.,* **55,** 88–101.

——, ——, M. Newman, J. D. Glick, and J. E. Schemm, 2000: Medium-range forecast errors associated with active episodes of the Madden–Julian oscillation. *Mon. Wea. Rev.,* **128,** 69–86.

Higgins, R. W., and K. C. Mo, 1997: Persistent North Pacific circulation anomalies and the tropical intraseasonal oscillation. *J. Climate,* **10,** 223–244.

Johnson, E. S., and M. J. McPhaden, 1993: On the structure of intraseasonal Kelvin waves in the equatorial Pacific Ocean. *J. Phys. Oceanogr.,* **23,** 608–625.

Johnson, G. C., M. J. McPhaden, and E. Firing, 2001: Equatorial Pacific Ocean horizontal velocity, divergence, and upwelling. *J. Phys. Oceanogr.,* **31,** 839–849.

Kessler, W. S., and M. J. McPhaden, 1995: The 1991–93 El Niño in the Central Pacific. *Deep-Sea Res.,* **42B,** 295–334.

——, and R. Kleeman, 2000: Rectification of the Madden–Julian oscillation into the ENSO cycle. *J. Climate,* **13,** 3560–3575.

——, M. J. McPhaden, and K. M. Weickmann, 1995: Forcing of intraseasonal Kelvin waves in the equatorial Pacific. *J. Geophys. Res.,* **100,** 10 613–10 631.

Kirtman, B. P., and P. S. Schopf, 1998: Decadal variability in ENSO predictability and prediction. *J. Climate,* **11,** 2804–2822.

Kutsuwada, K., and M. J. McPhaden, 2002: Intraseasonal variations in the upper equatorial Pacific Ocean during the 1997–98 El Niño. *J. Phys. Oceanogr.,* **32,** 1133–1149.

Lukas, R., and E. Lindstrom, 1991: The mixed layer in the western equatorial Pacific Ocean. *J. Geophys. Res.,* **96,** 3343–3357.

Madden, R. A., and P. R. Julian, 1994: Observations of the 40–50 day tropical oscillation—A review. *Mon. Wea. Rev.,* **122,** 814–847.

McPhaden, M. J., 1982: Variability in the central equatorial Indian Ocean. Part II: Oceanic heat and turbulent energy balance. *J. Mar. Res.,* **40,** 403–419.

——, 1999: Genesis and evolution of the 1997–98 El Niño. *Science,* **283,** 950–954.

——, and R. A. Knox, 1979: Equatorial Kelvin and inertio-gravity waves in zonal shear flow. *J. Phys. Oceanogr.,* **9,** 263–277.

——, and B. A. Taft, 1988: On the dynamics of seasonal and intraseasonal variability in the eastern equatorial Pacific. *J. Phys. Oceanogr.,* **18,** 1713–1732.

——, and X. Yu, 1999: Equatorial waves and the 1997–98 El Niño. *Geophys. Res. Lett.,* **26,** 2961–2964.

——, and Coauthors, 1998: The Tropical Ocean Global Atmosphere (TOGA) observing system: A decade of progress. *J. Geophys. Res.,* **103,** 14 169–14 240.

Moore, A. M., and R. Kleeman, 1999: Stochastic forcing of ENSO by the intraseasonal oscillation. *J. Climate,* **12,** 1199–1220.

Moore, D. W., and S. G. H. Philander, 1977: Modeling the tropical ocean circulation. *The Sea—Ideas and Observations on Progress in the Study the Seas,* Edward D. Goldberg, Ed., Marine Modeling, Vol. 6, Wiley and Sons, 319–361.

Payne, R. E., 1972: Albedo of the sea surface. *J. Atmos. Sci.,* **29,** 959–970.

Philander, S. G. H., 1979: Equatorial waves in the presence of the Equatorial Undercurrent. *J. Phys. Oceanogr.,* **9,** 254–262.

——, and Coauthors, 1985: Long waves in the equatorial Pacific Ocean. *Eos, Trans. Amer. Geophys. Union,* **66,** 154.

Ralph, E. A., K. Bi, P. P. Niiler, and Y. du Penhoat, 1997: A Lagrangian description of the western equatorial Pacific response to the wind burst of December 1992. *J. Climate,* **10,** 1706–1721.

Reed, R., 1977: On estimating insolation over the ocean. *J. Phys. Oceanogr.,* **7,** 482–485.

Reynolds, R. W., and T. M. Smith, 1994: Improved global sea surface temperature analysis using optimum interpolation. *J. Climate,* **7,** 929–948.

Shinoda, T., and H. H. Hendon, 1998: Mixed layer modeling of intraseasonal variability in the tropical western Pacific and Indian Oceans. *J. Climate,* **11,** 2668–2685.

——, ——, and J. Glick, 1998: Intraseasonal variability of surface fluxes and sea surface temperature in the tropical western Pacific and Indian Oceans. *J. Climate,* **11,** 1685–1702.

Slingo, J. M., and Coauthors, 1996: Intraseasonal oscillations in 15 atmospheric general circulation models: Results from an AMIP diagnostic subproject. *Climate Dyn.,* **12,** 325–357.

Sprintall, J., and M. Tomczak, 1992: Evidence of the barrier layer in the surface layer of the Tropics. *J. Geophys. Res.,* **97,** 7305–7316.

——, and M. J. McPhaden, 1994: Surface layer variations observed in multiyear time series measurements from the western equatorial Pacific. *J. Geophys. Res.,* **99,** 963–979.

Stevenson, J. W., and P. P. Niiler, 1983: Upper ocean heat budget during the Hawaii-to-Tahiti Shuttle Experiment. *J. Phys. Oceanogr.,* **13,** 1894–1907.

Takayabu, Y. N., T. Iguchi, M. Kachi, A. Shibata, and H. Kanzawa, 1999: Abrupt termination of the 1997–98 El Niño in response to a Madden–Julian oscillation. *Nature,* **402,** 279–282.

Waliser, D. E., K. M. Lau, and J.-H. Kim, 1999a: The influence of coupled sea surface temperatures on the Madden–Julian oscillation: A model perturbation experiment. *J. Atmos. Sci.,* **56,** 333–358.

——, C. Jones, J.-K. E. Schemm, and N. E. Graham, 1999b: A statistical extended-range forecast model based on the slow evolution of the Madden–Julian oscillation. *J. Climate,* **12,** 1918–1939.

Wang, B., and S. P. Xie, 1998: Coupled modes of the warm pool system. Part I: The role of air–sea interaction in maintaining Madden–Julian oscillation. *J. Climate,* **11,** 2116–2135.

Wang, W., and M. J. McPhaden, 1999: The surface layer heat balance in the equatorial Pacific ocean. Part I: Mean seasonal cycle. *J. Phys. Oceanogr.,* **29,** 1812–1831.

——, and ——, 2000: The surface layer heat balance in the equatorial

Pacific ocean. Part II: Interannual variability. *J. Phys. Oceanogr.*, **30,** 2989–3008.
——, and ——, 2001a: Surface layer heat balance in the equatorial Pacific Ocean during the 1997–98 El Niño and the 1998–99 La Niña. *J. Climate,* **14,** 3393–3407.
——, and ——, 2001b: What is the mean seasonal cycle of surface heat flux in the equatorial Pacific? *J. Geophys. Res.,* **106,** 837–857.
Webster, P. J., and R. Lukas, 1992: TOGA COARE: The Coupled Ocean–Atmosphere Response Experiment. *Bull. Amer. Meteor. Soc.,* **73,** 1377–1416.
Weller, R. A., and S. P. Anderson, 1996: Surface meteorology and air–sea fluxes in the western equatorial Pacific warm pool during TOGA COARE. *J. Climate,* **9,** 1959–1990.
Yu, X., and M. J. McPhaden, 1999: Seasonal variability in the equatorial Pacific. *J. Phys. Oceanogr.,* **29,** 925–947.
Zhang, C., 2001: Intraseasonal perturbations in sea surface temperatures of the equatorial eastern Pacific and their association with the Madden–Julian oscillation. *J. Climate,* **14,** 1309–1322.
——, and M. J. McPhaden, 2000: Intraseasonal surface cooling in the equatorial western Pacific. *J. Climate,* **13,** 2261–2276.
——, H. H. Hendon, W. S. Kessler, and A. J. Rosati, 2001: A workshop on the MJO and ENSO. *Bull. Amer. Meteor. Soc.,* **82,** 971–976.